CHARACTERIZATION OF $La_{1-x}Sr_x MnO_3$ ($0 \leq X \leq 0.2$) NANOPOWDERS SYNTHESIZED BY DIFFERENT METHODS

Faiçal DJANI[1], Ikram NOUREDDINE[1], Arturo MARTINEZ ARIAS[2]

Lanthanum manganite ($LaMnO_3$) partially substituted with Sr in the site A ($0 \leq x \leq 0.2$) were prepared by different synthesis methods (sol-gel, sol-gel combustion and auto-combustion) using citric acid or glycine as complexant or fuels and water as solvent. Thermogravimetric analysis technique (TGA) was used to explore precursor decomposition and to establish adequate calcination temperature for achievement of the perovskite structure in the nanoparticles. The samples obtained after calcination at 800°C were characterized by XRD, FTIR, PSD, and UV-Vis. Structural and vibration/electronic characteristics were examined on such basis and as a function of the preparation method employed.

Keywords: $LaMnO_3$, sol-gel, auto-combustion, TGA. XRD. FTIR, powder size distribution

1. Introduction

Perovskite mixed oxides with the general formula ABO_3 containing rare earth elements (in A position) and 3d transition metals (in B position) are considered as strategic materials due to their interesting electrical, magnetic, optical and catalytic properties [1-4]. Among them, manganese perovskites have been largely studied for sixty years and their rich variety of properties have shown to be useful for a number of applications (electronics, depollution, fuel cells, biomedical field, etc.) [4,5]. Manganites are mixed oxides of manganese which crystalizes in perovskite structure, and whose broad stoichiometric formula is $ABO_{(3\pm\delta)}$, where A is a lanthanide element and B is manganese. Among the ABO_3 perovskite structure, they could present an ideal cubic structure of P_{m3m} space group as well as structures belonging to orthorhombic P_{bnm} space group or rhombohedral R_{3CH} space group [6]. In recent years, lanthanum manganites ($La_{1-x}Sr_xMnO_3$) with unique electrical, magnetic and catalytic properties have attracted increasing interests for their applications in solid oxide fuel cells [7], giant magneto resistance [8] and catalytic combustion [9-11].

[1] Laboratory of Molecular Chemistry and Environment, University of Biskra, Biskra, Algeria, e-mail: fayssaldjani@yahoo.com

[2] Instituto de Catálisis y Petroleoquímica, CSIC, C/Marie Curie 2, Campus de Cantoblanco, Madrid, Spain

They can be synthesized by different methods. Typically, sol–gel techniques are employed although they could be required the use of expensive alkoxides as raw materials and need long time reaction. In turn, sol-gel combustion is a combination of the chemical sol–gel process and the combustion process; it constitutes fast, simple fast, simple and economic synthesis process to prepare nanometric powders. On the other hand, auto-combustion technique uses simple precursors and also constitutes a fast, simple and economic way to prepare this type of materials [12]. Within this context, in this work we have investigated the effect of synthesis method and dopant concentration on different physico-chemical properties of lanthanum strontium manganites $La_{1-x}Sr_xMnO_3$.

2. Experimental

2.1 Material synthesis

$La_{1-x}Sr_xMnO_3$ ($0 \leq x \leq 0.2$) mixed oxides were synthesized by three methods: sol-gel (S.G), sol-gel combustion (S.G.C) and auto-combustion (Au.C).

$La(NO_3)_3.6H_2O$, $Mn(NO_3)_2.4H_2O$, $Sr(NO_3)_2.6H_2O$ (Sigma Aldrich) and citric acid monohydrate $C_6H_8O_7$, glycine CH_2NH_2COH (Sigma-Aldrich) and distilled water were used as reagents and solvent, respectively. Stoichiometric amounts of $Sr(NO_3)_2.6H_2O$, $La(NO_3)_2.6H_2O$ and $Mn(NO_3)_2.4H_2O$ based on the composition of $La_{1-x}Sr_xMnO_3$ ($0 \leq x \leq 0.2$) were dissolved in distilled water. In addition to simple sol-gel citrate method using a known quantity of ethylene glycol with citric acid in order to increase the homogeneity of the solution and help to do a poly-condensation process in sol-gel method while in turn using ammonia with citric acid to adjust the pH to 7.0 is the strategy followed for sol-gel combustion method. Finally, the auto-combustion employing glycine as fuel is also explored as a third preparation method.

2.1.1 Synthesis of $LaMnO_3$ by a sol-gel method

Aqueous solutions of citric acid and of the metal nitrates were prepared separately and then mixed together and agitated for 2 h. The resulting solution was concentrated by slowly evaporating the water at 84°C until a gel was obtained. This gel was then dried slowly in an oven upon increasing the temperature to 100°C, and this temperature was maintained overnight in order to produce a solid amorphous citrate precursor. This precursor solid was finally calcined in air at 800°C for 5 h.

2.1.2 Synthesis of $LaMnO_3$ by a sol-gel combustion method

The appropriate amounts of metal nitrates and citric acid were first dissolved in distilled water. The pH value of the mixed solution was adjusted to 7.0 by adding a small amount of ammonia, obtaining a pink solution. Then, the solution was heated to 86°C for 62 min on a hot plate with continuous stirring for

dehydration. During dehydration process, poly-condensation reaction happened between citric acid and nitrates, which leads to formation of mentioned pink gel. The gels were put in an oven at 130°C during 24 h. Then, the gel was placed in a hot plate at 300°C. After a few minutes, the gels were ignited and burnt in a self-propagating combustion manner until all gels were completely burnt out to form a loose product [13]. The resulting precursor was finally calcined in air at 800°C for 5 h.

2.1.3 Synthesis of $La_{1-x}Sr_xMnO_3$ ($0 \leq x \leq 0.2$) by auto-combustion method

Aqueous solutions of glycine and of the metal nitrates were prepared separately and then mixed together with agitation. The mixture is heated between 50 to 60 minutes until achieving combustion with formation of cinders. The resulting products are submitted to grinding until we had a fine powder. The obtained solid precursors were finally calcined in air at 800°C for 5 h.

2.2 Characterization

Thermogravimetric and differential thermal analyses (TGA–DTA) of the precursor decomposition were performed on a Perkin Elmer TGA7 and Perkin Elmer DTA7 devices, respectively, from 20 to 900°C at a heating rate of 20 °C min^{-1} and under an air flow of ca. 60 mL min^{-1}.

X-ray diffraction (XRD) patterns were collected on a Bruker AXS D8 Advance diffractometer employing Cu Kα radiation. In all diffractograms, a step size of 0.028 (2 h) was used with a data collection time of 15 s. Data were collected between 2θ values of 10° and 80° using standard θ/2θ geometry. Identification of crystalline phases was carried out by comparison with JCPDS standards. The unit cell parameters were obtained by fitting the peak position of the XRD pattern using the Celref and X'pert Highscore programs.

Infrared transmission spectra were performed on a Fourier transform spectrometer (FTIR) Shimadzu 8400S. A granular technique employing KBr (1 mg of sample added to 200 mg of KBr) was used, and the spectra were recorded in the 400–4000 cm^{-1} range.

The analysis of the distribution of the grain size of the samples was employed in order to show the influence of the La/Sr substitution and the synthesis method employed on the particle size by laser granulometry. After calcination at 800°C, the powder was dispersed in deionized water in a beaker with magnetic stirring and combined under ultrasounds regime for 15 min. Powder size distribution (PSD) was characterized with a laser particle size analyzer (Mastersizer 2000, Malvern) [14].

Photocatalytic tests of samples prepared by different methods and different concentration of Sr where carried by testing the absorption at 264 nm using UV-visible spectrometer type Perkin Elmer Lambda 25 UV.

3. Results and discussion

One of the precursors (after the drying step of the preparation at 100 °C) was selected for its analysis by TGA–DTA in order to explore its decomposition under atmospheric air and with the aim of establishing most adequate calcination conditions for full decomposition and formation of corresponding perovskite. The results are shown in Fig. 1. Basically, four decomposition processes are identified. A first weight loss (ca. 11%) takes place between 23-150 °C which must be related to the desorption of adsorbed or hydration water which may remain in the precursors. The second one represents an important mass loss (ca. 69%). This step can account for most of the decomposition expected from the reaction involved in the whole process; $La(NO_3)_3 \cdot 6H_2O$ reacts with $Mn(NO_3)_2 \cdot 4H_2O$ and $C_6H_8O_7 \cdot H_2O$ and the products are $LaMnO_3 + N_2\uparrow + CO_2\uparrow + H_2O\uparrow$. It takes place between ca. 150 and 230 °C corresponding to the oxidative decomposition of citrates complexing the metals in the precursors. The third step takes place between ca. 230 and 350 °C and corresponds to a mass loss of about 4%. It could be related to the decomposition of carbonate or carboxylate-type complexes. The final process occurs slowly between 350 and 730 °C with a weight loss (ca. 6%) and must correspond to the final exothermic crystallization of the oxides, with the slow decomposition of more persistent residual carbonate- or carboxylate-type species. Therefore, as applied during the synthesis described in experimental, the temperature 800°C appears most adequate calcinations temperature to achieve full decomposition of precursors and transformation to final mixed oxide product.

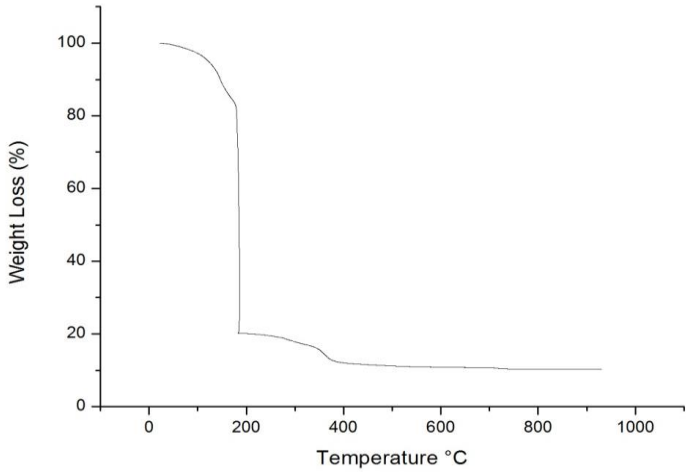

Fig.1. TGA curves during heating under air of the indicated powder precursors

The XRD powder patterns of $LaMnO_3$ prepared by three synthesis methods: sol-gel, sol-gel combustion and auto-combustion, calcined at 800°C, are shown in Fig.2. It shows the formation of perovskite phase with orthorhombic structure and Pbnm space group (JCPDS 00-035-1353) [16]. There is no important difference between the three XRD patterns although detailed analysis, as exposed in Table 1, reveals some subtle changes as a function of the preparation method employed.

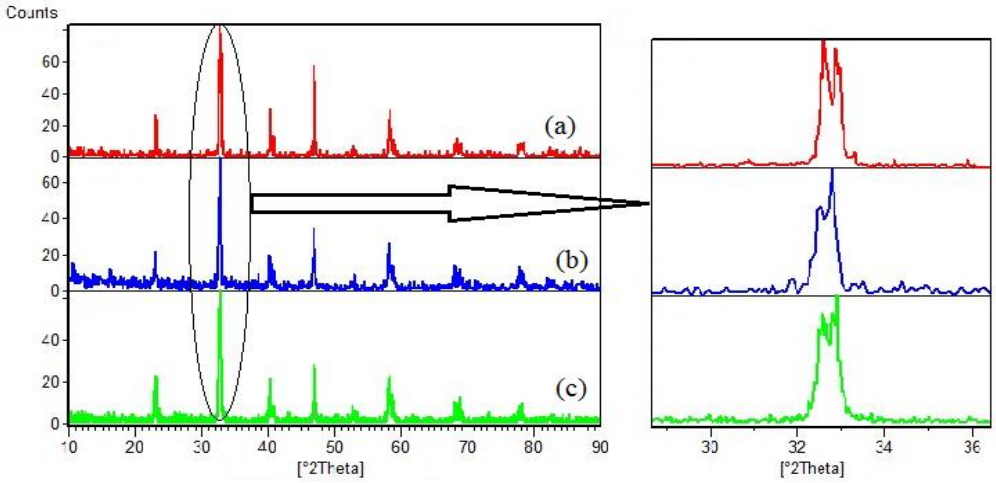

Fig.2. X-RD patterns of three samples $LaMnO_3$ calcined at 800°C, prepared by
(a) self-combustion, (b) sol-gel, (c) sol-gel combustion

Table1 shows the calculated structural information using the Celref and X'pert Highscore programs for the $LMnO_3$ samples.

Table 1

Refined lattice parameters for the $LaMnO_3$ samples

Synthesis method	Crystal system	a/Å	b/Å	c/Å	α/°	β/°	γ/°	V/Å	Space group
Sol-gel	Orthorhombic	5.5071	5.7432	7.7502	90	90	90	245.13	Pbnm
Sol-gel comb		5.5063	5.8231	7.7195	90	90	90	247.52	
Auto-combustion		5.4983	5.8183	7.7072	90	90	90	246.56	

The XRD powder patterns of $La_{1-x}Sr_xMnO_3$ ($0 \leq x \leq 0.2$) prepared by auto-combustion (samples calcined at 800 °C are shown in Fig.3. It shows the formation of perovskite phase with orthorhombic structure and Pbnm space group (JCPDS 00-035-1353) for x = 0. Replacement of Lanthanum by strontium ions in the perovskite A sites ($0 \leq x \leq 0.2$) causes a gradual decrease of the steric distortions and the structure changes from the orthorhombic (Pbnm) to rhombohedral R3-c symmetry (JCPDS 00-047-0444) for x = 0.1 and (JCPDS 00-053-0058) for x = 0.2 [17].

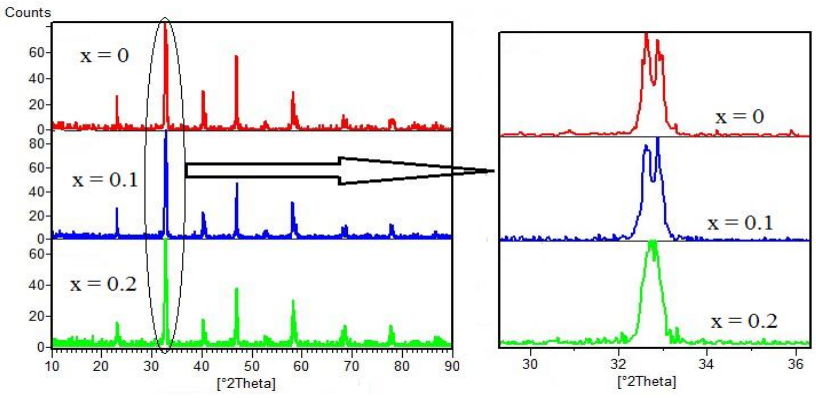

Fig.3. X-RD patterns of $La_{1-x}Sr_xMnO_3$ ($0 \leq x \leq 0.2$) calcined at 800°C (samples prepared by auto-combustion method)

Table 2 shows the calculated structural information using the Celref and X'pert Highscore programs for the $La_{1-x}Sr_xMnO_3$ ($0 \leq x \leq 0.2$) samples.

Table 2

Refined lattice parameters for the $La_{1-x}Sr_xMnO_3$ samples prepared by auto-combustion

Sample	Crystal system	a/Å	b/Å	c/Å	α/°	β/°	γ/°	V/Å	Space group
$LaMnO_3$	Ortho-rhombic	5.4983	5.8183	7.7072	90	90	90	246.56	Pbnm
$La_{0.9}Sr_{0.1}MnO_3$	Rhombo hedral	5.5064	5.5064	13.2951	90	90	120	349.11	R3-c
$La_{0.8}Sr_{0.2}MnO_3$		5.5021	5.5021	13.3174	90	90	120	349.15	

Figs. 4-6 exhibit infrared spectra for the samples. The absorption band at 610 cm^{-1} corresponds to a characteristic stretching mode, linked to the internal movement relative to a length change of the bands Mn-O associated with the octahedron MnO_6 [16]; it is attributed to a vibration characteristic of perovskite type ABO_3 structure [18-20]. As shown in Fig.5**,** this vibration appears practically at the same position for $LaMnO_3$ prepared by the different methods in good agreement with the analysis of X-ray diffraction results. However, there is a positive shift in the wavenumber of this absorption with increasing dopant concentration of Sr in La_{1-x} Sr_xMnO_3 (x=0.1 and x=0.2) oxides [21], as shown in Fig.6 and in consistency with the structural changes revealed by XRD.

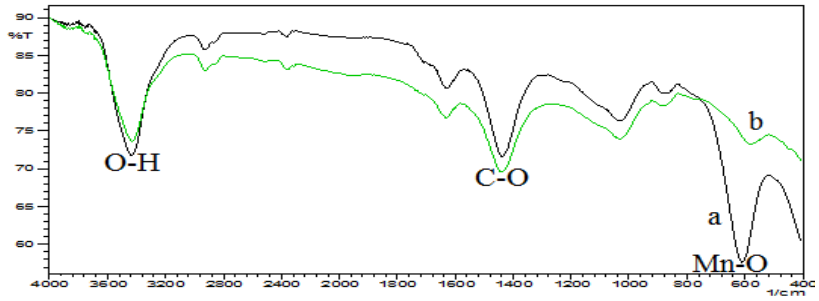

Fig.4. FT-IR spectra for $LaMnO_3$ prepared by auto-combustion method (a) after calcination, (b) before calcination

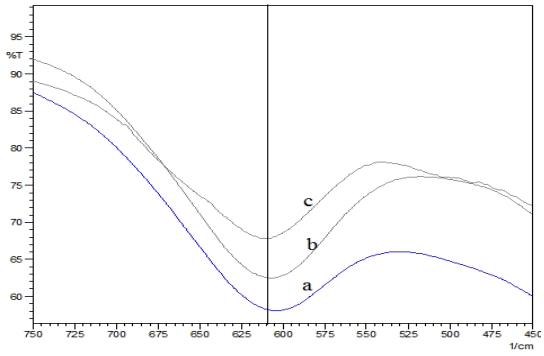

Fig.5. Mn-O stretching band of $LaMnO_3$ oxides (see main text) for samples calcined at 800°C and prepared by (a) auto-combustion, (b) sol-gel combustion, (c) sol-gel

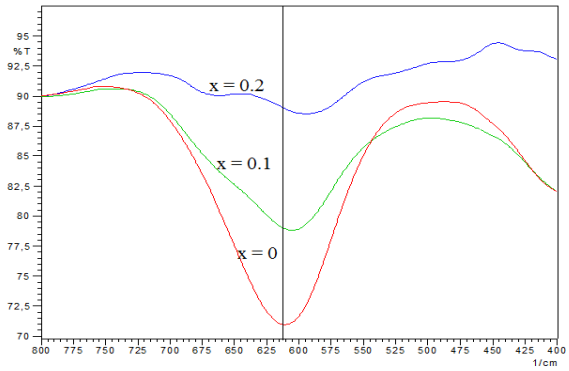

Fig.6. Mn-O stretching band (see main text) of the three $La_{1-x}Sr_xMnO_3$ oxides ($0 \leq x \leq 0.2$) prepared by auto-combustion (samples calcined at 800°C)

The grain size distributions of the different oxides calcined at 800°C, according to PSD measurements, are shown in Fig.7. The size distribution of the x=0, 0.1, 0.2 samples shows a maximum at ca. 0.178 microns. Data included in Table3 reveal that the particle size of $LaMnO_3$ prepared by sol-gel combustion (0.253 μm) is lower than that for the sample prepared by sol-gel (0.274 μm) or that prepared by auto-combustion (0.257 μm). Also, it is observed an increasing of particle size with increasing dopant concentration in Sr substituted $LaMnO_3$.The most homogeneous distribution appears that of the sample prepared by sol-gel; despite of multimodal distribution, peaks above 1 μm appear relatively small [6].

Table 3

The size distribution of mixed oxides prepared by different synthesis methods

Mixed oxide	**Synthesis method**	**Distribution of size**		
		d (0.1) (μm)	d (0.5) (μm)	d (0.9) (μm)
$LaMnO_3$	Auto-combustion	0.148	0.257	3.269
	Sol-gel combustion	0.148	0.253	2.933
	Sol-gel	0.149	0.274	4.110
$La_{0.9}Sr_{0.1}MnO_3$	Auto-combustion	0.144	0.227	0.803
$La_{0.8}Sr_{0.2}MnO_3$		0.149	0.297	7.181

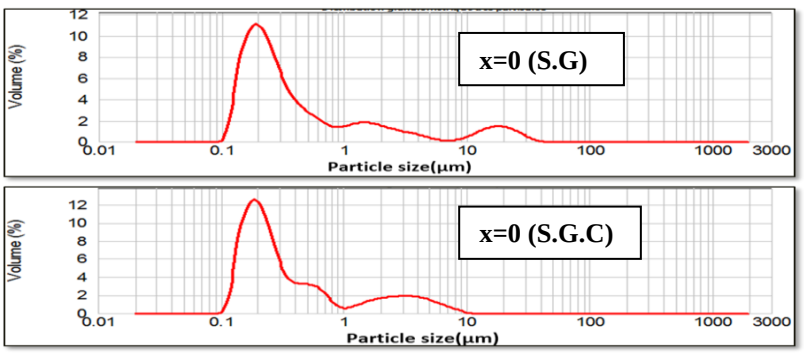

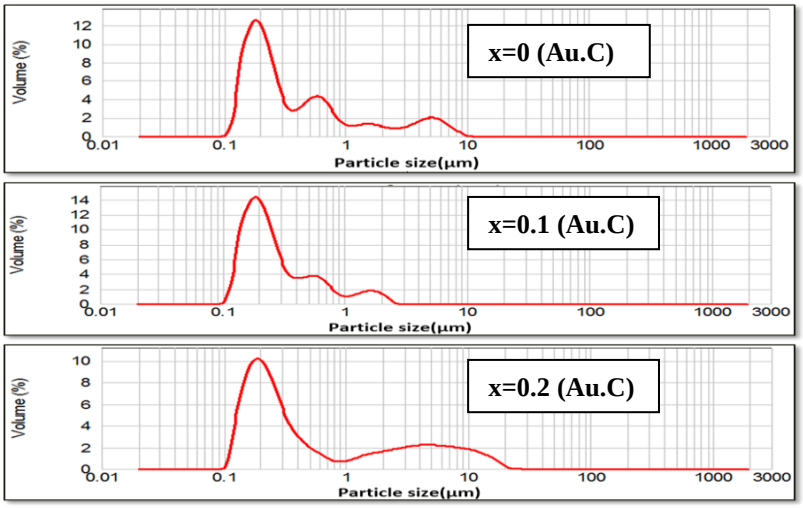

Fig.7 Particle size distribution of $La_{1-x}Sr_xMnO_3$ (0≤ x ≤0.2) oxides prepared by different methods

Uv-vis spectra for the samples are displayed in Figs. 8 and 9. They shows in all cases a maximum at wavelength λ_{max} = ca. 264 nm (as summarized in Table4); the profiles detected for the various compound indicate that the La_{1-x} Sr_xMnO_3 ($0 \leq x \leq 0.2$) compounds prepared by different synthesis methods present good potential as photocatalytic materials [12].

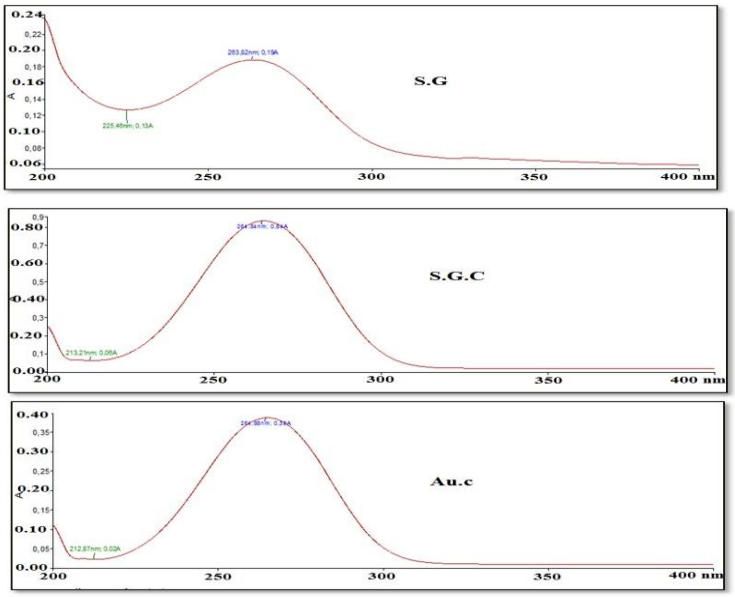

Fig.8 UV-vis spectra of the $LaMnO_3$ oxides prepared by different methods

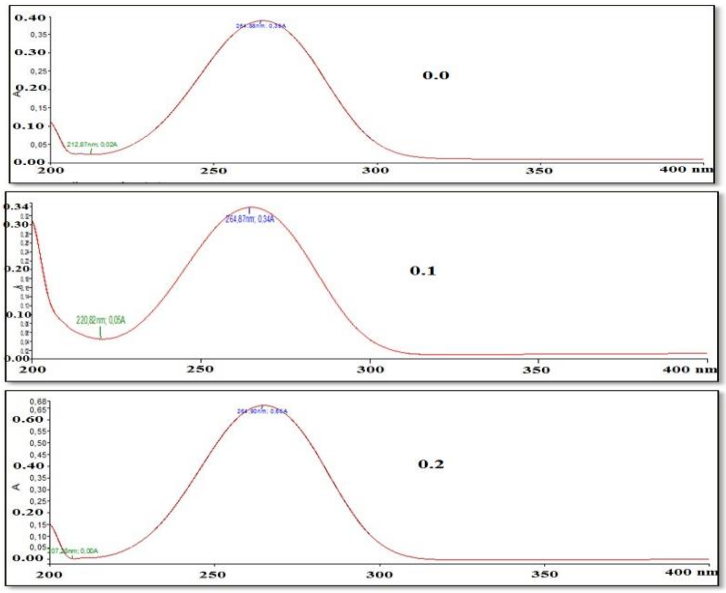

Fig.9 UV-Vis spectra of the $La_{1-x}Sr_xMnO_3$ oxides prepared by auto-combustion

Table.4

Maximum wavelength and absorbance of mixed oxides prepared by different synthesis methods according to UV-vis spectra

Mixed oxides	Synthesis Methods	Maximum wavelength (nm)	Maximum Absorbance
$LaMnO_3$	Auto-combustion	264.87	0.34
	Sol-gel combustion	264.84	0.84
	Sol-gel	263.82	0.19
$La_{0.9}Sr_{0.1}MnO_3$	Auto-combustion	264.88	0.39
$La_{0.8}Sr_{0.2}MnO_3$		264.90	0.66

4. Conclusions

In this work, our contribution focused on the synthesis and physicochemical characterization of $La_{1-x}Sr_xMnO_3$ ($0 \leq x \leq 0.2$) perovskite oxides. The thermo gravimetric analysis (TGA) allowed to identify the different transformations which take place during calcination under air of the solid precursors, temperatures at which synthesis precursors become decomposed as well as that of decomposition of other intermediate precursors, and final formation of the thermodynamically most favored final perovskite structure. This latter is

shown to starts from ca. 750°C, above which no further weight loss was detected, thus determining the stability range of the pure perovskite phase within the temperature range and under conditions studied. This is confirmed by the study by X-ray diffraction, in which it is shown that the samples calcined at 800°C exhibit the $La_{1-x}Sr_xMnO_3$ perovskite structure, irrespectively of the preparation method employed. XRD reveals the existence of the orthorhombic structure for $LaMnO_3$ samples which were prepared by three different synthesis methods and employing different fuel (glycine in auto-combustion; citric acid in the sol-gel combustion) and a complexing agent (citric acid in the sol-gel), with only subtle differences in structural parameters. For $La_{1-x}Sr_xMnO_3$ samples, when x increases the lattice parameters *a* and *b* tend to a single value related to achievement of the transition from orthorhombic phase → rhombohedral phase. The analysis by infrared spectroscopy of the samples showed an intense band at 610 cm^{-1} for $LaMnO_3$ prepared by three different synthesis methods as well as the perovskites doped with strontium, $La_{1-x}Sr_xMnO_3$ (x=0.1 and 0.2), in which a shift in such band was observed with the increase of x. The laser analysis of particle size has allowed us to follow the evolution of the oxide grains size, in which some differences appear as a function of the preparation method employed. Finally, examination of the $La_{1-x}Sr_xMnO_3$ perovskites by UV-vis spectroscopy reveals the presence of an absorption band at ca. 264 nm in all cases.

Acknowledgments

The ICP-CSCIC Unidad de Apoyo is acknowledged for the measurements of part of the characterization results.

R E F E R E N C E S

[1]. *P. Lacorre, J.B. Torrance, J. Pannetier, A.I. Nazzal, P.W. Wang, T.C. Huang*, Synthesis, crystal structure, and properties of metallic $PrNiO_3$: Comparison with metallic $NdNiO_3$ and semiconducting $SmNiO_3$, Journal of Solid State Chemistry, vol. 91, no 2, 1991, p. 225-237.

[2]. *M.S. Chen, T.B. Wu, J.M. Wu*, Effect of textured $LaNiO_3$ electrode on the fatigue improvement of Pb $(Zr_{0.53}Ti_{0.47})O_3$ thin films, Applied Physics Letters, vol. 68, no 10, 1996, p. 1430-1432.

[3]. *R.N. Singh, S.K. Tiwari, S.P. Singh, A.N. Jain, N.K. Singh*, Electrocatalytic activity of high specific surface area perovskite-type $LaNiO_3$ via sol-gel route for electrolytic oxygen evolution in alkaline solution, International J. of Hydrogen Energy, vol. 22, no 6, 1997, p. 557-562.

[4]. *M.A. Pena, J.L.G. Fierro*, Chemical structures and performance of perovskite oxides, Chemical Reviews, vol. 101, no 7, 2001, p. 1981-2018.

[5]. *R. Epherre*, Perovskites de manganese nanométriques: vers des applications biomedicales, Thèse de doctorat, Université Sciences et Technologies-Bordeaux I, 2010.

[6]. *E. Hernandez, V. Sagredo, G.E. Delgado*, Synthesis and magnetic characterization of LaMnO3 nanoparticles, Revista Mexicana de Física, vol. 61, no 3, 2015, p. 166-169.

[7]. *P. Holtappels, C. Bagger*, Fabrication and performance of advanced multi-layer SOFC cathodes, Journal of the European Ceramic Society, vol. 22, no 1, 2002, p. 41-48.
[8]. *E.L. Nagaev*, Colossal-magnetoresistance materials: manganites and conventional ferromagnetic semiconductors, Physics Reports, vol. 346, no 6, 2001, p. 387-531.
[9]. *A.E. Giannakas, A.K. Lavados, P.J. Pomonis*, Preparation, characterization and investigation of catalytic activity for NO+ CO reaction of $LaMnO_3$ and $LaFeO_3$ perovskites prepared via microemulsion method, Applied Catalysis B: Environmental, vol. 49, no 3, 2004, p. 147-158.
[10]. *R. Spinicci, M. Fatincanti, P. Marini, S. De Rossi, P. Porta*, Catalytic activity of $LaMnO_3$ and $LaCoO_3$ perovskites towards VOCs combustion, Journal of Molecular Catalysis A: Chemical, vol. 197, no 1, 2003, p. 147-155.
[11]. *S. Cimino, R. Pirone, L. Lisi*, Zirconia supported $LaMnO_3$ monoliths for the catalytic combustion of methane. Applied Catalysis B: Environmental, vol. 35, no 4, 2002, p. 243-254.
[12]. *Y. Li, S. Yao, L. Xue, Y. Yan*, Sol–gel combustion synthesis of nanocrystalline $LaMnO_3$ powders and photocatalystic properties, Journal of Materials Science, vol. 44, no 16, 2009, p. 4455-4459.
[13]. *Y. Li, L. Xue, L. Fan, Y. Yan*, The effect of citric acid to metal nitrates molar ratio on sol–gel combustion synthesis of nanocrystalline $LaMnO_3$ powders, Journal of Alloys and Compounds, vol. 478, no 1-2, 2009, p. 493-497.
[14]. *F. Djani, M. Omari, A. Martinez-Arias*, Synthesis, characterization and catalytic properties of La (Ni, Fe)O_3–NiO nanocomposites, Journal of Sol-Gel Science and Technology, vol. 78, no 1, 2016, p. 1-10.
[15]. *Z.M. Myat, T.T. Win, Y.M. Maung*, Investigation into electrospun $LaMnO_3$ nanofibres, Universities Research Journal, vol. 4, no. 4, 2011, p. 245-256.
[16]. *J. Wang, X. Zheng, X. Dong, Z. Qu, G. Liu, R. Xue, Y. Hao*, Synthesis of $LaMnO_3$ nanofibers via electrospinning, Applied Physics Research, vol. 1, no 2, 2009, p. 30-36.
[17]. *S. Vasseur, E. Duguet, J. Portier, G. Goglio, S. Mornet, E. Hadova, K. Knizek, M. Marysko, P. Veverka, E. Pollert*, Lanthanum manganese perovskite nanoparticles as possible in vivo mediators for magnetic hyperthermia, Journal of Magnetism and Magnetic Materials, 2006, vol. 302, no 2, 2006, p. 315-320.
[18]. *M.N. Iliev, A.P. Litvinchuk, M.V. Abrashev, V.G. Ivanov, H.-G. Lee, W.H. McCarroll, M. Greenblatt, R.L. Meng, C.W. Chu*, Raman monitoring of the dynamical Jahn-Teller distortions in rhombohedral antiferromagnetic $LaMnO_3$ and ferromagnetic magnetoresistive $La_{0.98}Mn_{0.96}O_3$, Physica C: Superconductivity, vol. 341-348, part 4, 2000, p. 2257-2258.
[19]. *L. Kebin, L. Xijun, Z. Kaigui, Z. Jingsheng, Z. Yuheng*, Infrared absorption spectra of manganese oxides, Journal Applied Physics, vol. 81, no. 10, 1997, p. 6943-6947.
[20]. *A.E. Lavat, E.J. Baran*, IR-spectroscopic characterization of $A_2BB'O_6$ perovskites, Vibrational Spectroscopy, vol. 32, no 2, 2003, p. 167-174.
[21]. *K. McBride J. Cook, S. Gray, S. Felton, L. Stella, D. Poulidi*, Evaluation of $La_{1-x}Sr_xMnO_3$($0 \leq x < 0.4$) synthesised via a modified sol–gel method as mediators for magnetic fluid hyperthermia, CrystEngComm, vol. 18, no 3, 2016, p. 407-416.